

Thermal X-ray Spectra of Supernova Remnants

Patrick Slane¹

¹Harvard-Smithsonian Center for Astrophysics
 60 Garden Street
 Cambridge, MA 02138 USA
 email: slane@cfa.harvard.edu

Abstract. The fast shocks that characterize supernova remnants heat circumstellar and ejecta material to extremely high temperatures, resulting in significant X-ray emission. The X-ray spectrum from an SNR carries a wealth of information about the temperature and ionization state of the plasma, the density distribution of the postshock material, and the composition of the ejecta. This, in turn, places strong constraints on the properties of the progenitor star, the explosive nucleosynthesis that produced the remnant, the properties of the environment into which the SNR expands, and the effects of particle acceleration on its dynamical evolution. Here I present results from X-ray studies SNRs in various evolutionary states, and highlight key results inferred from the thermal emission.

Keywords. (ISM:) supernova remnants, X-rays: ISM

1. Introduction

The very fast shocks formed in young and middle-aged supernova remnants (SNRs) act to heat matter to temperatures exceeding many millions of degrees. As a result, these systems are copious emitters of thermal X-rays. This emission, characterized by bremsstrahlung continuum accompanied by line emission from recombination and de-excitation in the ionized gas, can originate from three distinct regions of the SNR: (1) behind the forward shock (FS), where interstellar or circumstellar material is swept-up and heated; (2) interior to the SNR boundary, where cold ejecta are heated by the reverse shock (RS); and (3) outside a central pulsar wind nebula (PWN), if one exists, where the slow-moving central ejecta are heated by the expanding nebula. Thermal X-ray spectra in an SNR thus provide crucial information on the surrounding environment, which may have been modified by strong stellar winds from the progenitor, as well as the ejecta that bears the imprint of the stellar and explosive nucleosynthesis in the progenitor star.

Studies of the thermal X-ray emission from SNRs reveal details on the temperature, density, composition, and ionization state of the shocked plasma. These, in turn, can provide specific information on the density structure for both the ejecta and the surrounding circumstellar material, the nature of the supernova explosion (core-collapse vs. Type Ia), the age and explosion energy of the SNR, the mass of the progenitor star, and the distribution of metals in the post-explosion supernova. Here I present a summary of results from several studies of the thermal spectra of SNRs. This review is brief; space prohibits an in-depth discussion of many aspects and results from this rich field. For an excellent review of X-ray emission from SNRs, including a detailed discussion of the thermal X-ray emission, the reader is referred to Vink et al. (2012).

2. X-rays from SNRs

Spectral analysis of thermal X-ray emission can provide measurements of the electron temperature and the relative abundances in the shocked plasma. These quantities are important for studies of the dynamical evolution of the SNR and the composition of the shocked gas. However, the low density environments in which SNRs evolve result in crucial effects that affect the interpretation of the spectra. Of particular importance are the relatively long timescales for electron-ion temperature equilibration and ionization equilibrium.

2.1. Electron-Ion Temperature Equilibration

In the simplest picture, and for an ideal gas, all particles that go through the SNR shock attain a velocity $v = 3v_s/4$ where v_s is the shock velocity. Since the associated kinetic temperature scales with mass, the result is that the electron temperature is initially much lower than that of the ions. Because the ions comprise the bulk of the mass swept up by the SNR, it is the ion temperature that characterizes the dynamical evolution. However, the temperature determined from X-ray measurements is that of the electrons. Thus, in connecting X-ray measurements to the SNR evolution, modeling of the electron-ion temperature ratio is required.

On the slowest scales, Coulomb collisions between electrons and ions will bring the populations into temperature equilibrium. More rapid plasma processes may result in faster equilibration, and often the two extreme cases of instantaneous temperature equilibration and Coulomb equilibration are considered in order to investigate the boundaries of the problem. SNR expansion velocities can be used to estimate the ion temperatures for some remnants, and the estimated temperatures are much higher than the observed electron temperatures, suggesting slow temperature equilibration. However, the effects of cosmic-ray acceleration can result in ion temperatures lower than are indicated by the shock velocity (see Section 5), making more direct measurements of both T_e and T_i crucial.

In a small number of cases, measurements of Balmer lines at the forward shock can provide the proton temperature and the degree of electron-ion equilibration, and there is a significant trend for larger T_e/T_p values with lower shock velocities, potentially consistent with electron heating by lower hybrid waves (Ghavamian et al. 2007). Future high-resolution X-ray measurements of thermal line broadening offer the promise of direct measurements of both T_e and T_p in SNRs.

2.2. Ionization Effects

Because the density of the X-ray emitting plasma in SNRs is extremely low, the ionization state of the gas takes considerable time to reach the equilibrium state that is characteristic of its temperature. The ionization parameter $\tau = n_e t$ determines how far the ionization has progressed. The plasma reaches collisional ionization equilibrium (CIE) for $\tau \gtrsim 10^{12.5} \text{ cm}^{-3} \text{ s}$; for smaller values the plasma is in a nonequilibrium ionization (NEI) state. This is illustrated in Figure 1. The left panel shows a portion of the soft X-ray spectrum for a plasma at a temperature of $10^{6.5} \text{ K}$ for different values of $n_e t$. Of particular note is the relative strengths of the O VII triplet and the Ly α and Ly β lines from O VIII. It is clear from this that determination of the plasma temperature based on relative line strengths must thus account for NEI conditions in the plasma. In the right panel, we plot the same spectra folded through the *Chandra* ACIS-S detector response. While the limited spectral resolution provided by CCD detectors obviously obscures details of specific line ratios, spectral fits to the spectrum can easily identify gross differences of the ionization state.

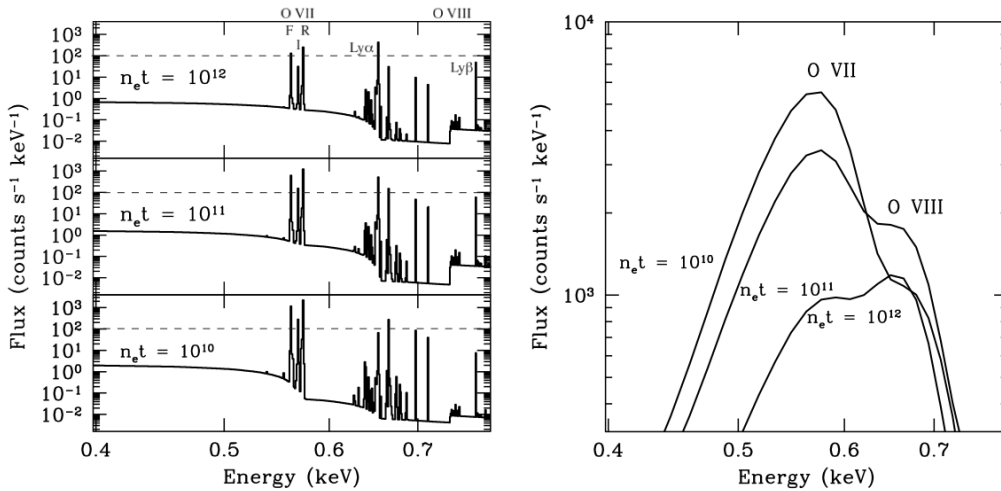


Figure 1. Left: Evolution of X-ray spectrum with ionization age, emphasizing lines from O VII and O VIII. The plasma temperature is $10^{6.5}$ K, and the units for $n_e t$ are $\text{cm}^{-3} \text{s}^{-1}$. The dashed line at 10^2 counts $\text{s}^{-1} \text{keV}^{-1}$ is simply for comparison purposes. Right: Spectra at left folded through the *Chandra* ACIS-S detector response.

The progression of the ionization state in the evolving postshock gas in SNRs is readily observed. Early *Chandra* observations of 1E 0102.2–7219, for example, show that the peak of the O VII emission is found at a smaller radius than that of O VIII, consistent with the expectation that the ionization state of ejecta most recently encountered by the inward-propagating RS lags behind that of the ejecta that have been shocked earlier (Gaetz et al. 2000). The same effect is evident in shocked circumstellar material in G292.0+1.8, where the ionization state of the emission directly behind the FS is observed to be considerably lower than that for regions further downstream (Lee et al. 2010). Such measurements thus provide constraints on the thermal history of the shocked material as well as on variations in the density structure.

While conditions of underionization are found in many SNRs, recent X-ray observations have identified exactly the opposite situation in several remnants. Kawasaki et al. (2005) used the relative intensity of H-like and He-like lines of Ar and Ca from *ASCA* observations of W49B to determine an ionization temperature that is higher than T_e , indicating an *overionized* plasma. Ozawa et al. (2009) used *Suzaku* observations to identify a distinct radiative recombination continuum (RRC) feature that confirms this overionized state (Figure 2, left). Using *XMM* observations, Miceli et al. (2010) find that the overionization in W49B appears to be related to regions in which rapid expansion and adiabatic cooling have lowered the plasma temperature to a value below its ionization state. Similar results have been observed for IC 443 (Yamaguchi et al. 2009). A semi-quantitative analysis by Moriya (2012) suggests that the progenitors of such overionized SNRs may be massive RSG stars for which the wind-driven circumstellar environment is sufficiently dense to promote rapid early ionization followed by a drop in temperature as the SNR expands into the lower density regions of the wind shell. This is illustrated in Figure 2 (right) where the electron density encountered by a $10,000 \text{ km s}^{-1}$ shock traveling through a CSM formed by a stellar wind is shown. The dashed line follows regions for which the plasma will reach approximate ionization equilibrium. The shaded region corresponds to mass-loss rates typical of a massive RSG progenitor, and shows that for early times, the plasma may be left in an overionized state. Such conditions

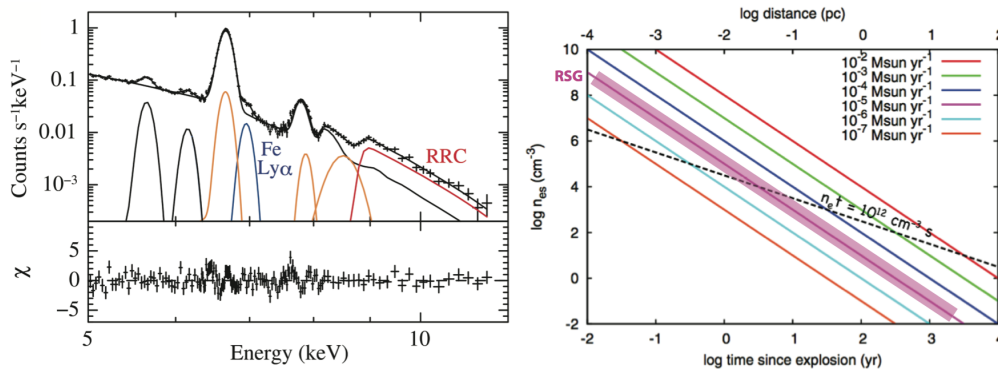


Figure 2. Left: *Suzaku* spectrum for W49B, showing RRC features and enhanced H-like emission from Fe, indicative of overionized plasma. (From Ozawa et al. 2009.) Right: Electron density distribution for wind model as a function of time (and distance) traveled by $10,000 \text{ km s}^{-1}$ SNR shock. See text for description. (From Moriya 2012. Reproduced by permission of the AAS.)

appear to be connected to the mixed-morphology class of SNRs, making further study of the dynamical conditions leading to such overionized states of particular interest.

3. Studies of SNR Ejecta

The very different stellar evolution histories and explosion processes for Type Ia and core-collapse (CC) SNe result in distinct signatures in the shock-heated ejecta of SNRs. Type Ia events, corresponding to the complete disruption of a C/O white dwarf star, produce more than $0.5M_{\odot}$ of Fe-group elements, accompanied by a significant contribution of intermediate mass elements. CC SNe, on the other hand, are dominated by materials synthesized during the stellar evolution of the massive progenitor – particularly O – with additional products from explosive nucleosynthesis in the innermost regions surrounding the collapsed core. As illustrated in Figure 3 (left), where we plot the mass distributions for key nucleosynthesis products for characteristic Type Ia and CC events (Iwamoto et al. 1999), the former are dominated by Fe while the latter contain much larger amounts of O. For comparison, the total mass of these elements contained in $10M_{\odot}$ of swept-up material with solar abundances is also shown. Particularly at young ages when the total amount of mass swept up by the FS is not exceedingly high, the thermal X-ray spectra from such remnants provide rich information about supernova ejecta.

In Figure 3 (right), we compare the spectra from N103B (top), a Type Ia SNR (Lewis et al. 2003) with that from the CC SNR G292.0+1.8 (bottom). The dominant flux just below 1 keV in N103B is largely from Fe-L emission, characteristic of the large amount of Fe created in such events, while the spectrum from G292.0+1.8 shows strong emission features from O and Ne (Park et al. 2004). Identification and modeling of such spectral features has been used to identify the SN type that produced numerous SNRs, notably Kepler’s SNR, which Reynolds et al. (2007) identified as a Type Ia remnant based on the dominant Si, S, and Fe emission. Subsequent detection and modeling of the Mn and Cr lines in Kepler imply a high-metallicity progenitor star (Park et al. 2013).

A particularly important example of SNR “typing” through X-ray spectra is that of SNR 0509–67.5. Hughes et al. (1995) used *ASCA* spectra to argue for a Type Ia progenitor for this remnant. By comparing different Type Ia explosion models with spectra from *XMM* and *Chandra* observations, Badenes et al. (2008) argued that 0509–67.5 is

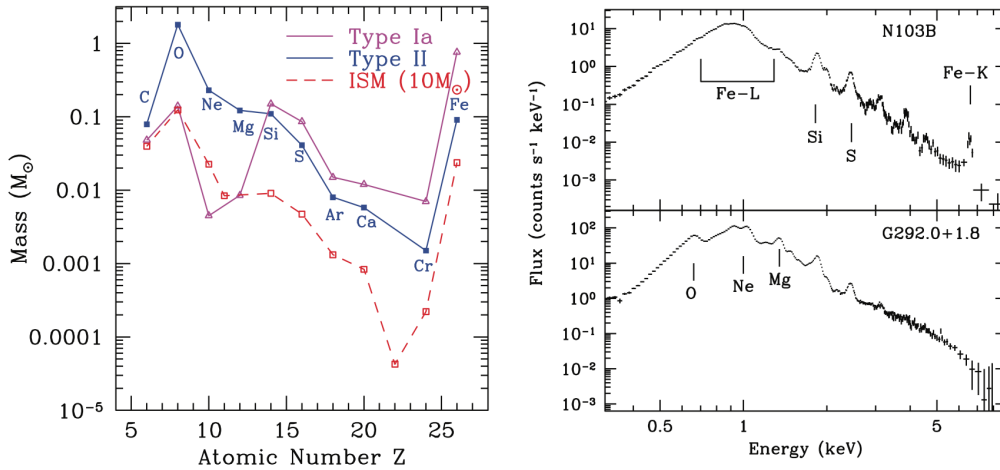


Figure 3. Left: Mass of ejecta components, by atomic number, in representative core-collapse and Type Ia SNe. For comparison, the mass contained in $10M_{\odot}$ of solar-abundance material is also shown. Right: Thermal X-ray spectra from a Type Ia remnant (N103B) and core-collapse remnant (G292.0+1.8), illustrating the significant difference in Fe and O/Ne content.

the result of an energetic, high-luminosity SN 1991T-like event, a result subsequently confirmed with light echo spectra from the original event (Rest et al. 2008).

The early development of SN explosions can imprint signatures on the SNRs that they form. Studies of the spatial distribution of ejecta can thus provide evidence of asymmetries and mixing in these events. X-ray studies of Cas A, for example, show distinct evidence of Fe ejecta in the outermost regions of the remnant (Hughes et al. 2000a), despite the expectation that Fe is produced in the regions closest to the remnant core. This large-scale disruption of the ejecta layers has been studied in detail by Hwang and Laming (2012) who performed fits to over 6000 X-ray spectra in Cas A and find distinct examples of regions where Fe is accompanied by other products of incomplete Si burning, along with others that are nearly pure Fe, presumably produced in regions of α -rich freezeout during complete Si burning. They conclude that nearly all of the Fe in Cas A is found outside the central regions of the remnant, apparently the result of hydrodynamic instabilities in the explosion.

The large-scale distribution of SNR ejecta has been investigated for a large number of SNRs by Lopez et al. (2011), who find that the thermal X-ray emission from remnants of Type Ia events shows a higher degree of spherical symmetry and mirror symmetry than for CC remnants. This may indicate that CC SNe evolve in more asymmetric environments, or perhaps that the events themselves are asymmetric.

4. Studies of Shocked Circumstellar Material

Remnants of CC SNe initially evolve in the circumstellar environment left by their associated progenitors. For progenitors with significant pre-explosion wind phases, the remnants initially evolve into density profiles with $\rho \propto r^{-2}$. The composition of the circumstellar material from progenitors with strong RSG or WR wind episodes is expected to show the signatures of the CNO cycle, which leads to an environment with an enhanced N/O ratio. Studies of thermal X-ray emission from behind the FS can provide constraints on the shocked CSM, and thus on the late-phase properties of the progenitor star.

Detection of enhanced N in a shocked CSM environment is complicated by both in-

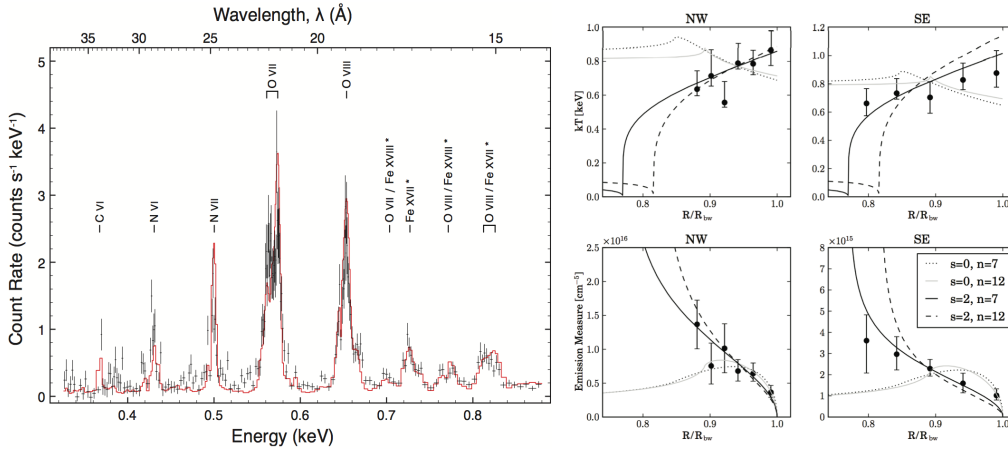


Figure 4. Left: *XMM* RGS spectrum from G296.1–0.5 showing N and O line features from shocked circumstellar wind. (From Castro et al. 2011.) Right: Temperature and emission measure profiles of FS regions in G292.0+1.8 compared with power law density models for uniform ($s = 0$) and wind-like ($s = 2$) surroundings, and ejecta profiles typical of Type Ia ($n = 7$) and CC ($n = 12$) events. (From Lee et al. 2010.) [Figures reproduced by permission of the AAS.]

terstellar absorption and the modest spectral resolution provided by typical X-ray CCD detectors. *XMM* spectra of G296.1–0.5 from the MOS and pn detectors reveal emission from regions just behind the FS that indicate a low column density and weak evidence for an overabundance of N and an underabundance of O, as expected from CNO-cycle products found in winds of massive stars. High resolution spectroscopy using the *XMM* RGS (Figure 4, left) confirm these results, clearly establishing the remnant as the result of a CC event from a fairly massive progenitor (Castro et al. 2011). Using the similarity solution of Chevalier (2005), the inferred swept-up wind mass is $\sim d_2^{5/2} 19 M_\odot$, and the SNR age is $\sim 2800 E_{51}^{-1/2} d_2^{9/4}$ yr.

G292.0+1.8 is an O-rich SNR with an identified pulsar and PWN, clearly establishing it as the result of a CC event. X-ray spectral studies suggest a progenitor mass of $\sim 20 - 40 M_\odot$ (Hughes & Singh 1994; Gonzalez & Safi-Harb 2003; Park et al. 2004), making it likely that the remnant has evolved in the stellar wind density profile of its progenitor. *Chandra* studies of the thermal X-ray emission from the outer regions of the SNR shell (Figure 4, right) reveal a temperature and emission measure structure consistent with predictions of the similarity solutions from Chevalier (2005) for evolution in a medium with $\rho \propto r^{-2}$, with a steep ejecta profile typical of CC events (Lee et al. 2010). The overall kinematics are consistent with evolution in an RSG wind comprising a mass of more than $15 M_\odot$. More recently, the same technique has been applied to the thermal X-ray emission from Cas A, revealing similar evidence of a circumstellar environment dominated by an RSG wind (Lee et al. – these proceedings).

5. Constraints on Particle Acceleration

Particle acceleration in SNRs has long been suggested as a primary source for production of Galactic cosmic-rays, and X-ray measurements have provided some of the most important constraints on this process. While much of this evidence is provided by synchrotron radiation, whose presence indicates the presence of multi-TeV electrons, significant information is provided by the thermal X-ray emission as well. In 1E 0102.2–7219, the temperature derived from X-ray measurements is much lower than that implied by the

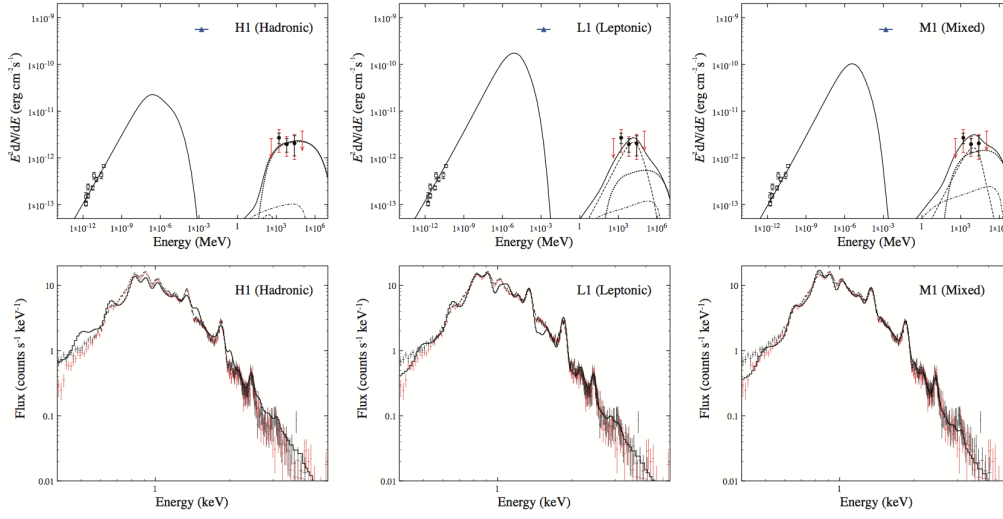


Figure 5. Broadband (upper) and thermal X-ray (lower) spectra from CTB 109 along with models in which the γ -ray emission is dominated by hadrons (left), electrons (center), and a mixture (right). The thermal X-ray spectra provides a best fit for the mixed scenario. (From Castro et al. 2012. Reproduced by permission of the AAS.)

shock velocity determined from expansion measurements, even accounting for the slowest possible equilibration between the electrons and ions (Hughes et al. 2000b). This result is consistent with a picture in which a significant fraction of the shock energy has gone into the acceleration of particles instead of heating the gas. In Tycho’s SNR, the separation between the FS and contact discontinuity (and also RS) is much smaller than predicted from dynamical models of the SNR evolution unless a significant amount of energy has been lost to some nonthermal process, such as particle acceleration (Warren et al. 2005). It is crucial to note that, since cosmic-ray protons outnumber electrons by a factor of ~ 100 , the significant energy in relativistic particles inferred from these studies provides strong evidence for acceleration of cosmic-ray *ions* in SNRs.

Observations of γ -ray emission from SNRs provide additional compelling evidence for particle acceleration. Because γ -rays can be produced by both electrons (though inverse-Compton scattering and nonthermal bremsstrahlung) and protons (though the production of neutral pions, which decay to γ -rays), modeling of the broadband emission is required to determine the origin of the γ -rays, and thus the total efficiency with which the systems are able to accelerate particles. In RX J1713.7–3946, hydrodynamical modeling of the SNR evolution that includes particle acceleration, and follows the ionization history of the postshock gas, shows that the *absence* of observed thermal X-ray emission places strong constraints on the ambient density, effectively ruling out significant π^0 -decay γ -rays (Ellison et al. 2010, 2012) for scenarios with expansion into a uniform medium or wind-driven cavity, although evolution in a medium with dense clumps may provide sufficient target material for a pions to provide a dominant contribution (Inoue et al. 2012).

In CTB 109, for which γ -ray emission is also observed, self-consistent modeling (Castro et al. 2012) of the evolution can produce broadband spectra that adequately reproduce the observed radio and γ -ray emission for scenarios in which hadrons dominate the γ -rays (Figure 5, left), or in which the γ -rays originate primarily from electrons (Figure 5, center). However, the thermal X-ray emission predicted by both of these models fails

to reproduce the observed *XMM* spectrum. The high density required for hadrons to dominate results in an overproduction of high ion states for Mg and Si, while the low density required for electrons to dominate results in an underprediction of the same ion states. A mixed scenario in which the density is sufficiently high for electrons and protons to contribute nearly equally to the γ -ray flux yields excellent agreement with the thermal X-ray emission.

6. Conclusions

As indicated in this brief review, thermal X-ray spectra from SNRs provide information on the nature, environments, and dynamical evolution of these systems. Current X-ray observatories continue to uncover new and important properties of both bright, nearby SNRs and the fainter population within the Galaxy and beyond. Advances in plasma codes, MHD simulations, and upcoming high spectral resolution capabilities that will become available with *ASTRO-H*, hold particular interest for enhancing our abilities to probe the detailed physics of SNRs and their evolution.

This work was carried out under support from NASA Contract NAS8-03060.

References

- Badenes, C. et al. 2008, *ApJ*, 680, 1149
 Castro, D. et al. 2011, *ApJ*, 734, 86
 Castro, D. et al. 2012, *ApJ*, 756, 88
 Chevalier, R. A. 2005, *ApJ*, 619, 839
 Ellison, D. C. et al. 2010, *ApJ*, 712, 287
 Ellison, D. C. et al. 2012, *ApJ*, 744, 39
 Gaensler, B. M. & Slane, P. 2006, *ARAAS*, 44, 17
 Gaetz, T. J. et al. 2000, *ApJ*, 534, L47
 Ghavamian, P. et al. 2007, *ApJ*, 654, L69
 Gonzalez, M. & Safi-Harb, S. 2003, *ApJ*, 583, L91
 Hughes, J. P. & Singh, K. P. 1994, *ApJ*, 422, 126
 Hughes, J. P. et al. 1995, *ApJ*, 444, L81
 Hughes, J. P. et al. 2000a, *ApJ*, 528, L109
 Hughes, J. P. et al. 2000b, *ApJ*, 543, L61
 Hwang, U., & Laming, J. M. 2012, *ApJ*, 746, 130
 Inoue, K. et al. 2012, *ApJ*, 744, 71
 Iwamoto, K. et al. 1999, *ApJS*, 125, 439
 Kawasaki, M. et al. 2005, *ApJ*, 631, 935
 Lee, J. J. et al. 2010, *ApJ*, 711, 861
 Lewis, K. T. et al. 2003, *ApJ*, 582, 770
 Lopez, L. A. et al. 2011, *ApJ*, 732, 114
 Miceli, M. et al. 2010, *A&A*, 514, L2
 Moriya, T. J. 2012, *ApJ*, 750, L13
 Ozawa, M. et al. 2009, *ApJ*, 706, L71
 Park, S. et al. 2004, *ApJ*, 602, L33
 Park, S. et al. 2013, *ApJ* (in press; arXiv:1302.5435)
 Rest, A. et al. 2008, *ApJ*, 680, 1137
 Reynolds, S. P. et al. 2007, *ApJ*, 668, L135
 Vink, J. 2012, *A&AR*, 20, 49
 Warren, J. S. et al. 2005, *ApJ*, 634, 376
 Yamaguchi, H. et al. 2009, *ApJ*, 705, L6